NASA TECHNICAL NOTE

NASA TN D-2587

NASA TN D-2587

EXPERIMENTAL EFFECTS OF PROPELLANT-INTRODUCTION MODE ON ELECTRON-BOMBARDMENT ION ROCKET PERFORMANCE

by Paul D. Reader

Lewis Research Center

Cleveland, Ohio

NATIONAL AERONAUTICS AND SPACE ADMINISTRATION • WASHINGTON, D. C. • JANUARY 1965

EXPERIMENTAL EFFECTS OF PROPELLANT-INTRODUCTION MODE ON ELECTRON-BOMBARDMENT ION ROCKET PERFORMANCE

By Paul D. Reader

Lewis Research Center
Cleveland, Ohio

NATIONAL AERONAUTICS AND SPACE ADMINISTRATION

For sale by the Office of Technical Services, Department of Commerce,
Washington, D.C. 20230 -- Price $1.00

EXPERIMENTAL EFFECTS OF PROPELLANT-INTRODUCTION MODE ON ELECTRON-BOMBARDMENT ION ROCKET PERFORMANCE

by Paul D. Reader

Lewis Research Center

SUMMARY

An investigation was undertaken to determine the effects of propellant-introduction mode on the ion-chamber and accelerator-system performance of electron-bombardment ion rockets. The location of the propellant-inlet apertures in the walls of the ion chamber were varied in an attempt to obtain a more uniform ion-current-density profile at the screen grid, as well as an improved ionization efficiency. Several 10- and 20-centimeter-diameter ion sources were used to verify the trends encountered experimentally over a range of thrustor geometries.

Introduction of propellant vapor near the accelerator system and at the periphery of the cylindrical ion chamber resulted in both lower discharge power losses and more uniform accelerator erosion when compared with a conventional through-flow propellant-introduction mode. The more uniform accelerator erosion that resulted from the peripheral-feed mode could extend the life of the accelerator system by as much as a factor of four.

INTRODUCTION

Research on electron-bombardment ion rockets of the type shown in figure 1 has resulted in a simple, reliable, and efficient unit. As shown in reference 1, the power loss associated with the magnetic field used to contain the discharge can be eliminated through the use of permanent-magnet circuits. The accelerator impingement has been reduced to a value near the level predicted by charge-exchange calculations (ref. 2). Several investigators have reported excellent progress in increasing the durability of the cathode (refs. 3 to 5). Further improvements in efficiency and durability appear possible, however, and would have significant effects on the ultimate mission capability of the thrustor. In an attempt to reduce ion-chamber power losses and electrode erosion, an investigation was undertaken to determine the effects of the mode of propellant injection on ion-chamber performance.

Beam-current-density measurements and accelerator-erosion patterns for the thrustor of figure 1 indicated that the center area, near the axis, contributes

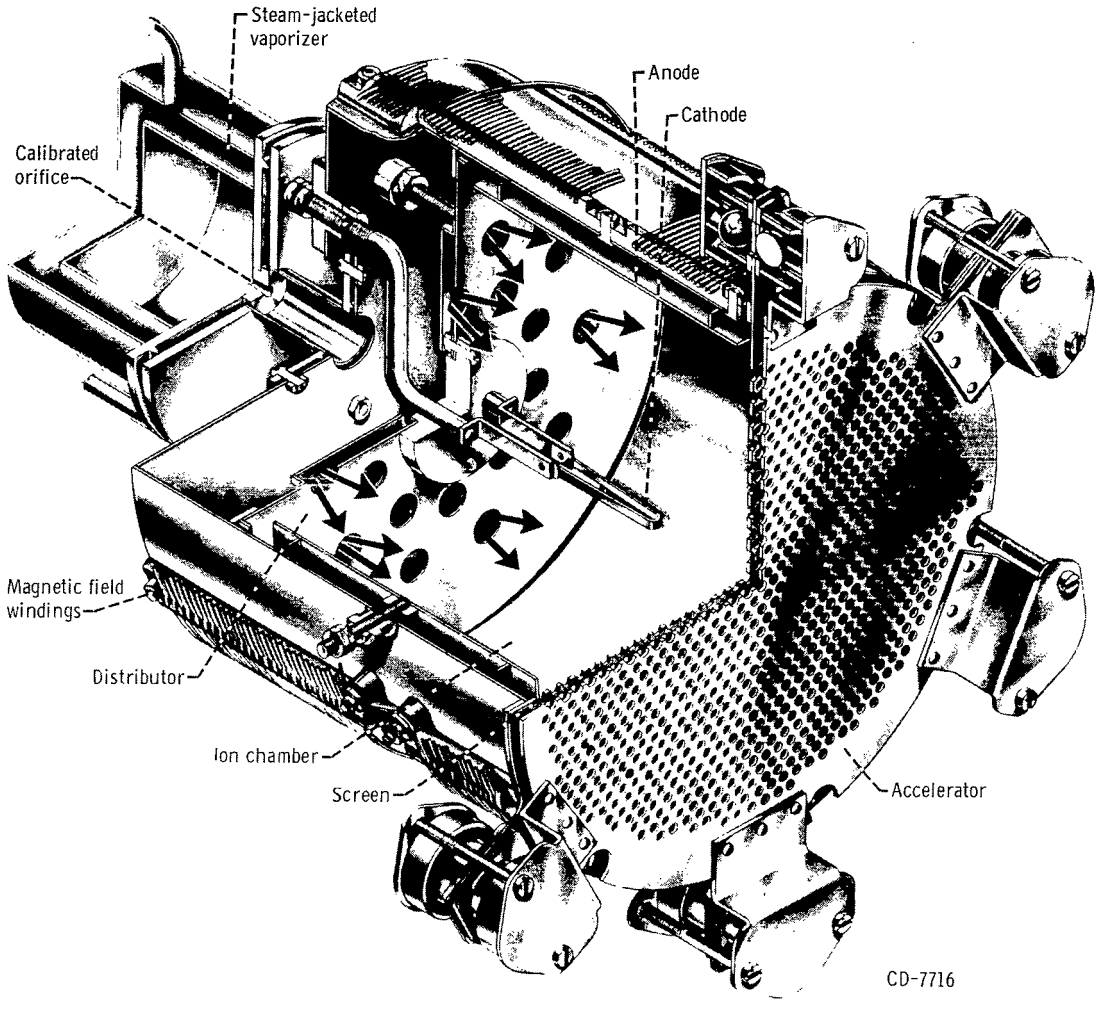

Figure 1. - Cutaway view of typical 20-centimeter-diameter electron-bombardment thrustor.

thrustor of figure 1 indicated that the center area, near the axis, contributes a major percentage of the total ion beam (ref. 6). This fact is not unexpected in view of the centrally located filament and the resulting radial distribution of high-velocity ionizing electrons. If a uniform ion-current profile could be obtained at the screen grid, the resulting uniform accelerator erosion would allow the useful life of the accelerator grid system to be increased by a factor of about four. Conversely, if the initial duration was adequate, a uniform current profile would allow the current density to be about doubled for the given accelerator lifetime (ref. 2).

There are two possible methods of producing a more uniform ion-current profile. The first is to use several cathodes distributed around the ion chamber; this method would be both mechanically and electrically complex. The second method is to offset the lower density of ionizing electrons near the anode by introducing the propellant at this location, which would thereby tend to produce a more uniform ion density at the plane of the accelerator system. The second method was followed in the present investigation.

A number of propellant-injector designs were incorporated into several 10- and 20-centimeter-diameter electron-bombardment ion sources of otherwise conventional design. The location and the shape of the propellant-introduction apertures in the walls of the chamber were varied in an attempt to minimize ion-chamber power losses. Discharge power losses and accelerator electrode-erosion patterns were measured for these propellant-introduction modes, and the results are compared with those for previously conceived through-feed designs.

APPARATUS

Thrustors

A cutaway view of a typical electron-bombardment ion rocket is shown in figure 1. The propellant flow rate is controlled by a calibrated orifice between the vaporizer and the flow distributor. After leaving the distributor, the flow enters the ion chamber, where the propellant is bombarded with electrons from the cathode. The solenoidal windings surrounding the ion chamber provide an approximately axial magnetic field, which increases the probability of electron-propellant collisions by preventing the rapid escape of electrons to the anode. Escape of electrons to the ends of the chamber is prevented by operating these ends at the same potential as the cathode. Some of the propellant is ionized by the bombarding electrons, and some of these ions arrive at the screen and are accelerated to produce an ion beam. A neutralizer (not shown in fig. 1) then current and charge neutralizes the ion beam.

The accelerating grids are match-drilled molybdenum plates. The remainder of the thrustor, with the exception of the filament, insulators, and field windings, was fabricated of nonmagnetic stainless steel.

An attempt was made throughout the investigation to maintain thrustor operation at a propellant-utilization efficiency of 80 percent. Temperature-control tolerances on the propellant vaporizer resulted in uncertainties in the flow rate of ±5 percent. These flow-variation tolerances appear as a spread in the data when the curves are cross-plotted. Most of this spread is well within the ±5-percent flow variation.

Figure 2 shows cutaway sketches of a 10-centimeter-diameter thrustor specifically designed for propellant-feed studies with the following modifications: conventional through feed (fig. 2(a)), cross feed (fig. 2(b)), angle feed, nominally 45° against the ion-beam flow (fig. 2(c)), and the final configuration, reverse feed (fig. 2(d)).

No significant attempt was made to optimize the geometric parameters (other than the mode of propellant injection) of the thrustor designed for these tests. The through-feed data were used as the performance baseline.

Two additional thrustors were employed in the program to verify the results of the tests on the unit shown in figure 2. One of these thrustors was 10 centimeters in diameter (as was the thrustor shown in fig. 2), and the other was 20 centimeters in diameter. A cutaway view of the second 10-centimeter

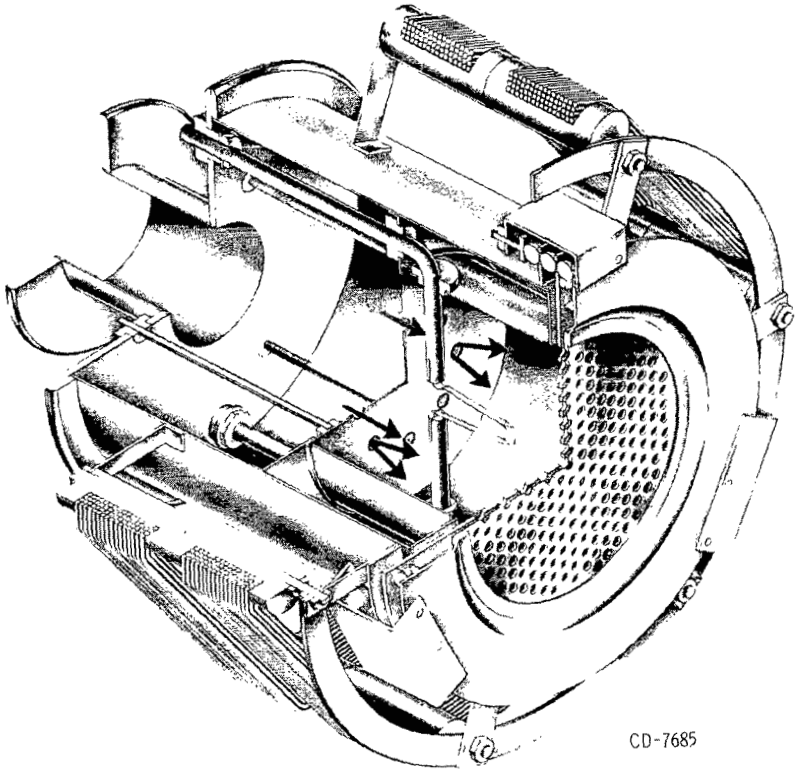

(a) Through feed.

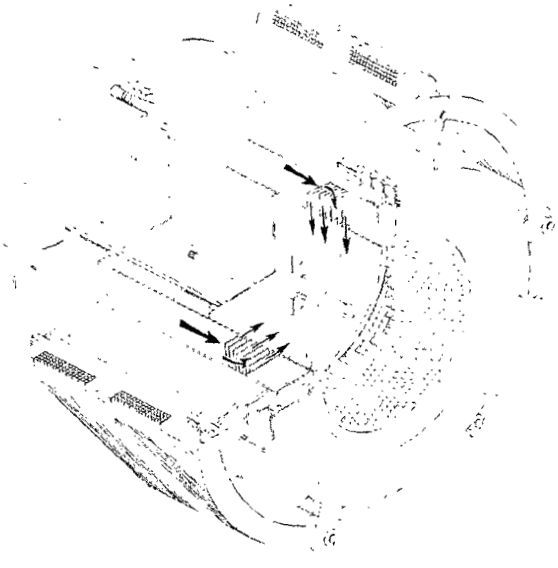

(b) Cross feed.

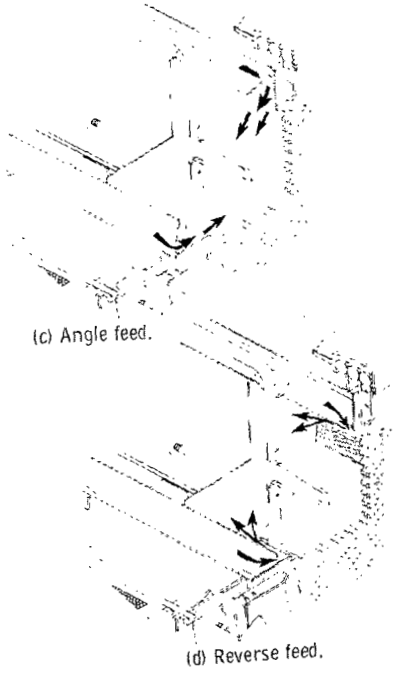

(c) Angle feed.

(d) Reverse feed.

Figure 2. - Cutaway view of first 10-centimeter-diameter thrustor showing various modifications.

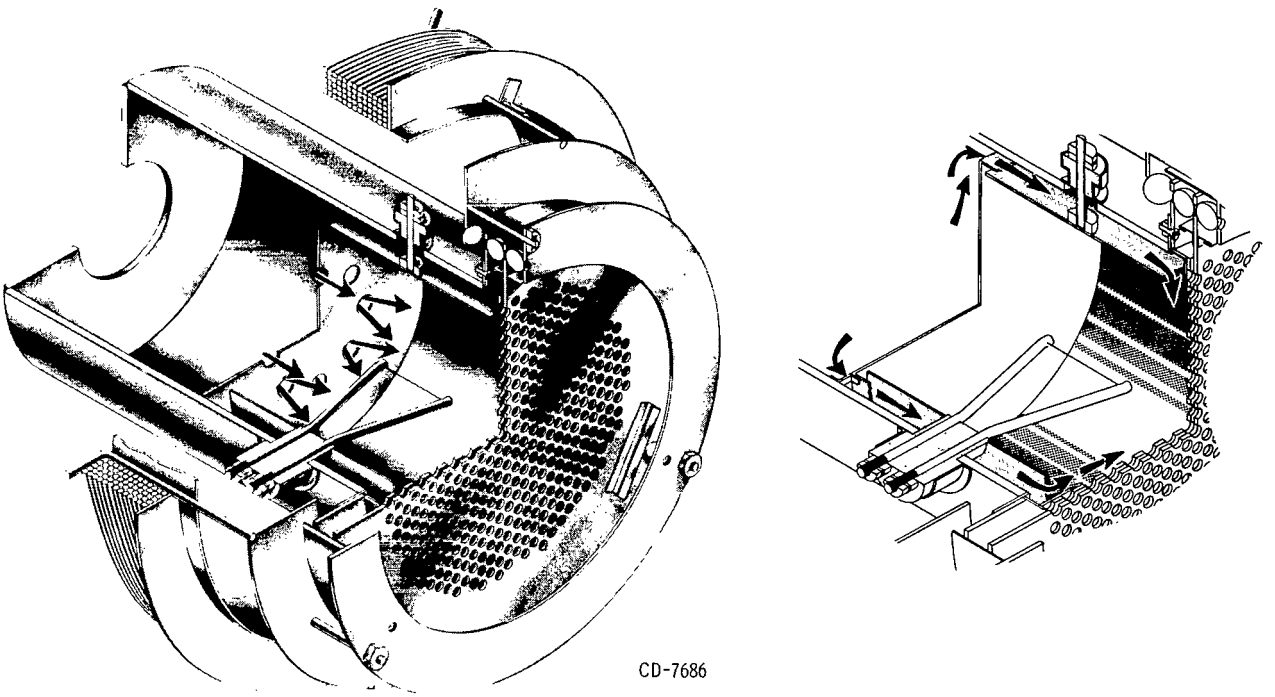

(a) Through feed. (b) Side feed.

Figure 3. - Cutaway view of second 10-centimeter-diameter thrustor showing conversion to side feed.

thrustor is shown in figure 3(a) in the through-feed configuration, with the modifications made to convert to a "side-feed" mode shown in figure 3(b). (The modified cross-feed system used on the second 10- and on the 20-centimeter-diameter thrustors will be referred to as "side feed" because the propellant is simply introduced through holes in the anode.)

The 20-centimeter-diameter thrustor was used to determine the effects of changing the size of the chamber and the feed system on ion-chamber performance.

The 20-centimeter-diameter thrustor is shown in figure 1 (p. 2), and the modifications to convert it from through to side feed are shown in figure 4.

Electrical System

The power-supply and metering system used during these tests is shown in schematic form in figure 5. The power supplies had ratings sufficiently high that all data taken were obtained with the same power supplies.

Facility

The installation of a thrustor in one of the 5-foot-diameter, 16-foot-long

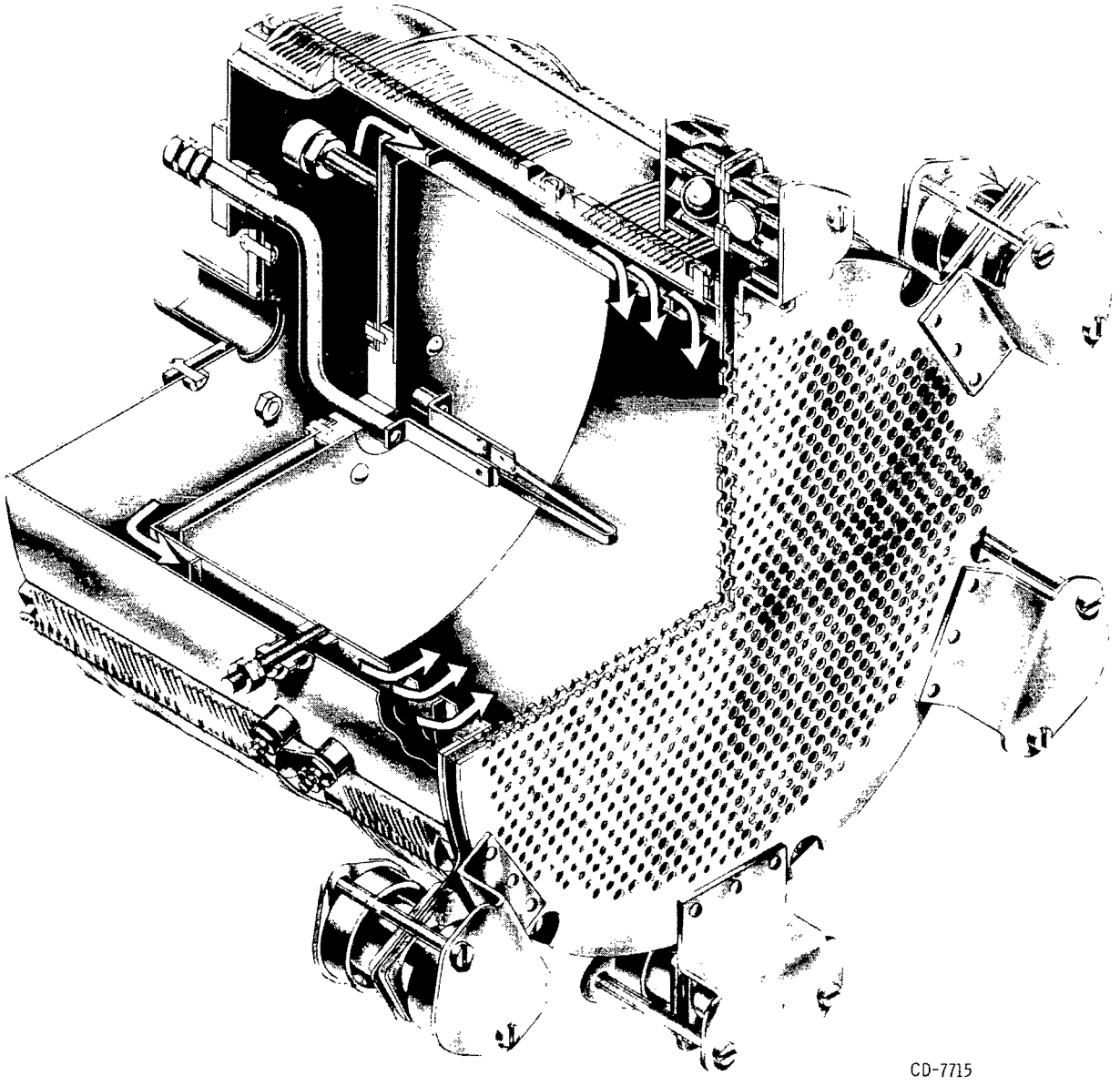

Figure 4. - Cutaway view of 20-centimeter-diameter thrustor converted to side-feed propellant-introduction mode.

vacuum tanks at the NASA Lewis Research Center is shown in figure 6. The tank has four 32-inch oil-diffusion pumps feeding into a common ejector pump, followed by a mechanical pump. With cryogenic pumping used in conjunction with the pumps, thrustor operation was possible at pressures of approximately 10^{-6} millimeter of mercury.

DISCUSSION OF RESULTS

The most common method of comparing the performance of several electron-

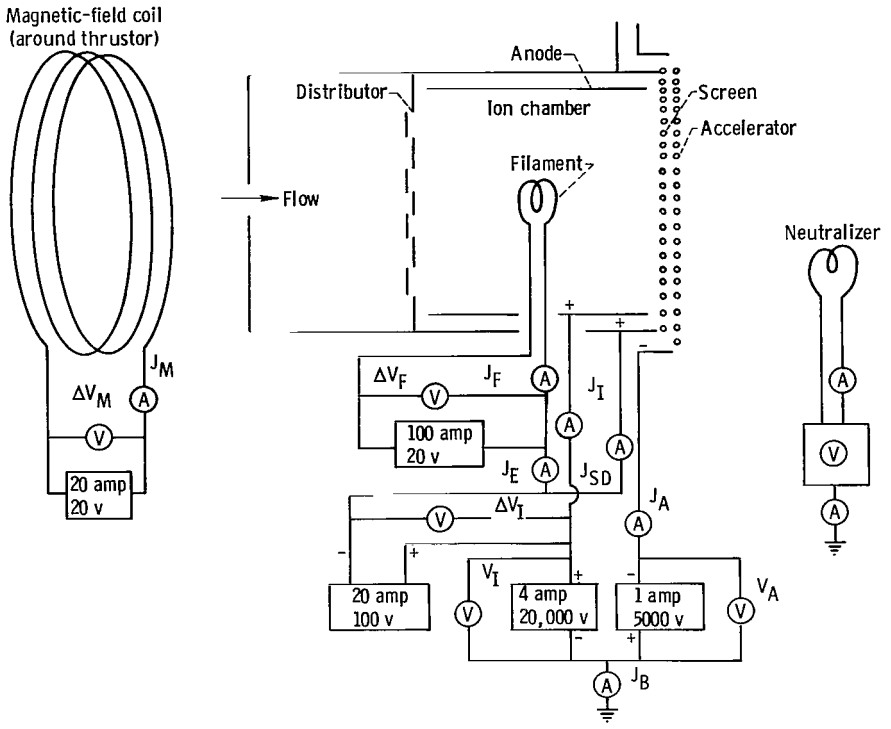

Figure 5. - Wiring diagram of electron-bombardment ion rocket.

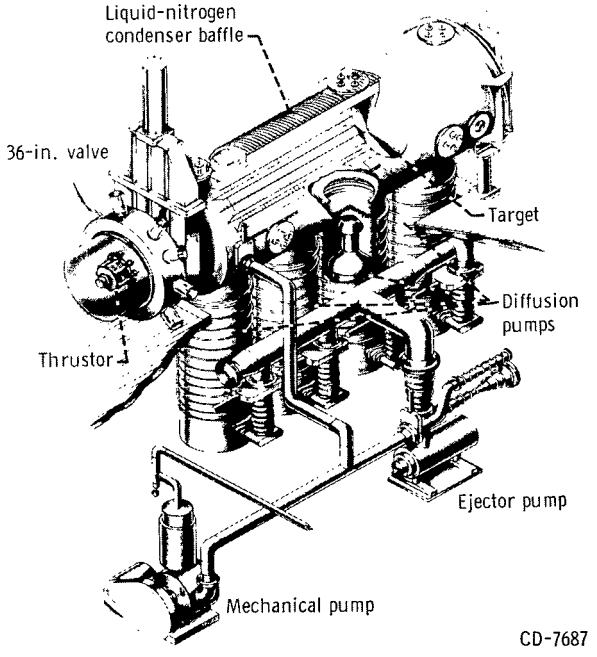

Figure 6. - Vacuum facility with thrustor installation.

bombardment ion sources is to determine the discharge energy required to produce a beam ion. In the source being considered this term is found by multiplying the discharge potential (ion-chamber potential difference) by the difference in the discharge (anode) and beam currents. The energy loss in electron volts per ion is then determined by dividing the power term mentioned previously by the beam current. The beam current is subtracted from the anode current to account for the low-energy secondary electrons liberated in the ionization process.

This energy-loss term will be used to compare the performance of several thrustors over ranges of electrical parameters with different propellant-distribution systems.

Comparison of Propellant-Introduction Directions

For a through-feed system the propellant enters through a distributor at one end of the cylindrical ion chamber and leaves (mostly as ions) through the screen and the accelerator grids at the other end (figs. 1, p. 2, and 2(a), p. 4). Since the accelerator system for the present study has a 50-percent-open area, there is a probability that some of the neutral propellant flow can pass directly through the chamber without striking the chamber walls (ref. 7). The fact that propellant-utilization efficiencies in the range of 90 to 95 percent can be obtained (by using sufficient discharge power) with the through-feed system indicates that the transit time across the ion chamber is sufficiently long to allow at least some of these "one-pass" atoms to become ionized.

Previous tests conducted with modifications of the through-feed propellant-feed method have shown moderate ion-chamber-performance variations with changes in the configuration of the distributor (ref. 8). Introducing the propellant at the screen in a direction nominally opposite the beam ion flow should cause the average mercury atom to make at least one more pass along the length of the chamber, which would effectively reduce the percentage of atoms that could escape directly without striking the chamber walls.

Introduction of the propellant at the periphery of the chamber in the vicinity of the screen grid should also tend to promote the rapid extraction of the ions that are formed in the region of high propellant density near the propellant-introduction apertures. As previously mentioned, the area of the grid system near the anode is relatively lightly loaded (lower current density) with the through-feed flow mode.

Similarly, if the direction of flow can be made approximately radial, the mean propellant-atom residence time in the chamber might increase before the random reflecting and scattering processes cause it to pass out of the chamber through the screen. The distribution modes shown in figures 2(b), (c), and (d) (p. 4) were fabricated to investigate these concepts of propellant injection.

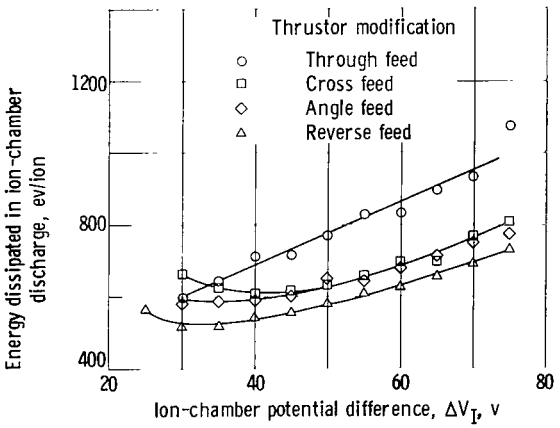

Figure 7. - Ion-chamber performance of 10-centimeter-diameter thrustor with several propellant-introduction modes. Net accelerating potential, 4000 volts; magnetic-field strength at screen, 33 gauss; accelerator potential, -2000 volts; beam current, 0.125 ampere.

Figure 7 is a performance comparison of the four propellant-feed methods shown in figure 2 (p. 4). The energy dissipated in the discharge per beam ion is plotted against the ion-chamber potential difference. The beam current from the 10-centimeter-diameter thrustor was 0.125 ampere at a specific impulse of 5000 seconds. The magnetic field at the screen was 33 gauss. The figure shows that the performance of the three feed systems in which the propellant is introduced at or near the screen grid on the periphery of the chamber is improved when

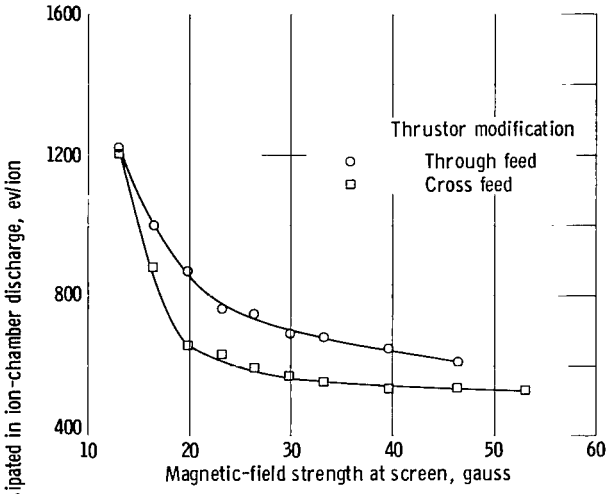

(a) Effect of magnetic-field strength on energy dissipated in ion-chamber discharge. Net accelerating potential, 4000 volts; ion-chamber potential difference, 40 volts.

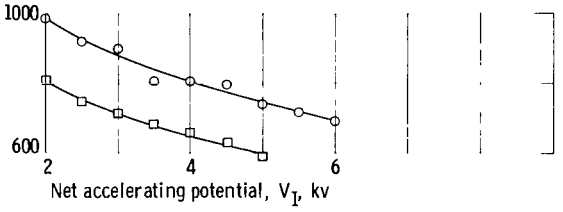

(b) Effect of net accelerating potential on energy dissipated in ion-chamber discharge. Ion-chamber potential difference, 50 volts; magnetic-field strength at screen, 33 gauss.

Figure 8. - Ion-chamber performance of 10-centimeter-diameter thrustor with through and cross feed. Accelerator potential, -2000 volts; beam current, 0.125 ampere.

compared with the conventional through-feed system near the normal-operating point of 50 volts.

Figure 8 shows the performance of the through-feed system compared with that of the cross-feed system when magnetic-field strength and net accelerating potential were varied. The performance of the angle- and the reverse-feed systems was near enough to the performance of the cross-feed system that inclusion of these data on the plot would only have obscured the curve. In general, the performance of the angle- and the reverse-feed modes was superior to that of the cross-feed system. All data for each feed system are included in tables I to III.

The variation of discharge losses with increasing magnetic-field strength is shown in figure 8(a). The value of field strength recorded is that on the axis of the ion chamber at the screen grid. The specific impulse was 5000 seconds and the beam current 0.125 ampere. The energy dissipated per beam ion drops rapidly with the increasing magnetic-field strength because of the improved containment of the high-velocity ionizing electrons. At about 30 gauss, the decreasing losses level out, and further increases in the field strength do not greatly benefit the ionization process. The trends displayed by both the through- and the cross-feed propellant-introduction modes are similar, but the cross-feed mode has lower discharge losses as well as a more well-defined transition from rapidly decreasing losses to fairly constant losses as the magnetic-field strength increases.

The influence of the net accelerating potential on the energy dissipated in the discharge per beam ion is indicated in figure 8(b). The beam current was 0.125 ampere with a discharge potential of 50 volts and a magnetic-field strength at the screen of 33 gauss. The drop in losses with increasing net accelerating potential was due to the increasing penetration of the electrostatic field back into the ion chamber, which thus aided the ion extraction process. The cross-feed configuration again exhibits superior ion-chamber performance over the range of net accelerating potentials.

With the magnetic field used to take the preceding data, the field strength at the screen was approximately 60 percent of that at the distributor. This decrease in field strength toward the screen benefits the ion-chamber per-

formance (ref. 9). The other thrustors used in the program had about the same field-strength ratios.

An optimum ion-chamber length for a 10-centimeter-diameter, through-feed configuration had previously been determined as being about 5 to 10 centimeters (ref. 9). A few short runs were made with the cross-feed propellant mode to determine the effects of varying the ion-chamber length on this system. The performance of the cross-feed system deteriorated slightly (10 percent) in going to either 5- or 10-centimeter chamber lengths from a 7.5-centimeter length. As a result of these tests, all data reported herein for 10-centimeter-diameter chambers were taken with an ion-chamber length of 7.5 centimeters. The length of the 20-centimeter-diameter chamber was maintained at 15 centimeters.

The performance of the through- and cross-feed systems are compared at a higher beam current and, hence, current density in figure 9. The 10-centimeter-diameter thrustor, the same used for the data of figures 7 (p. 8) and 8 (p. 9) and shown in figure 2 (p. 4), was operated at a beam current of 0.25 ampere.

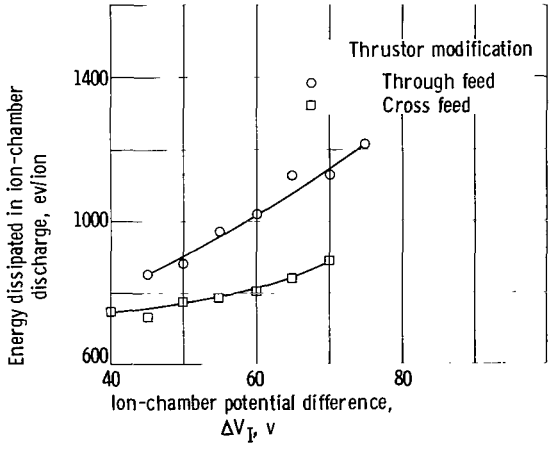

Figure 9. - Ion-chamber performance of 10-centimeter-diameter thrustor with through and cross feed. Beam current, 0.25 ampere; net accelerating potential, 4000 volts; accelerator potential, -2000 volts; magnetic-field strength at screen, 42 gauss.

The net accelerating potential was 4000 volts with the accelerator being operated at -2000 volts. The magnetic-field strength at the screen was 42 gauss. The cross-feed propellant-introduction mode again shows superior performance. A more gradual increase in losses with increasing ion-chamber potential difference is evident. The low-voltage end of each curve represents approximately the same emission limit of the filament type used for these tests and indicates one of the benefits derived from decreased ion-chamber losses. The more efficient cross-feed unit can be operated at ion-chamber potential differences 5 volts lower than the through-feed unit and can maintain the same propellant-utilization efficiency for the same cathode emission current (about 4 amp). This performance difference may allow the cross-feed unit to operate in a low range of ion-chamber (discharge voltage) potential differences and thus increase cathode durability (refs. 3 and 5).

Performance of Second 10-Centimeter-Diameter Source

In order to verify the trends displayed in figures 7 (p. 8) and 8 (p. 9) for a 10-centimeter-diameter source operating at a 0.125-ampere beam current, a second 10-centimeter source was tested. This source is shown in figure 3 (p. 5) and is very similar to the unit reported in reference 10. The source, shown in figure 3(a) in the through-feed propellant-flow configuration, had given the best performance of any unit operated in this propellant-feed mode.

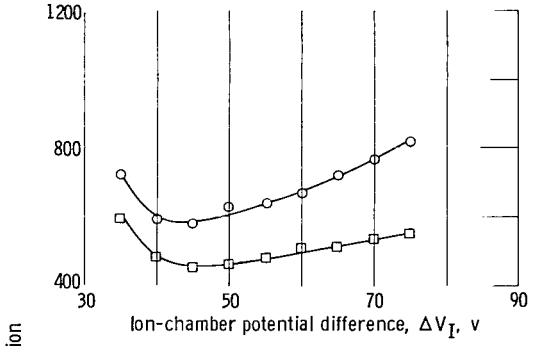

(a) Effect of ion-chamber potential difference on energy dissipated in ion-chamber discharge. Net accelerating potential, 4000 volts; magnetic-field strength at screen, 42 gauss.

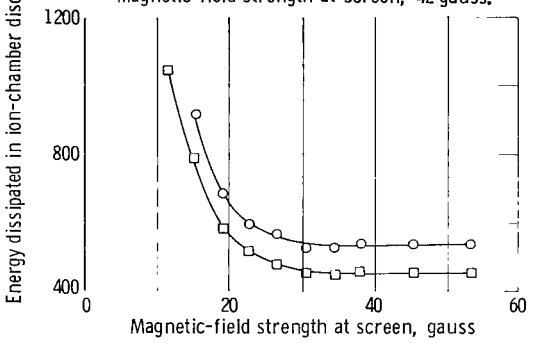

(b) Effect of magnetic-field strength on energy dissipated in ion-chamber discharge. Ion-chamber potential difference, 40 volts; net accelerating potential, 4000 volts.

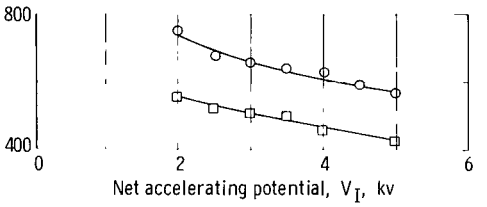

(c) Effect of net accelerating potential on energy dissipated in ion-chamber discharge. Ion-chamber potential difference, 50 volts; magnetic-field strength at screen, 42 gauss.

Figure 10. - Comparison of ion-chamber performance of second 10-centimeter diameter thrustor with side- and through-feed propellant flow. Accelerator potential, -2 kilovolts; beam current, 0.125 ampere; propellant-utilization efficiency, 0.8.

After data were taken with the through-feed system for comparison purposes, the thrustor was altered to approximate a modified cross-feed configuration as shown in figure 3(b).

The data obtained with these two feed modes are compared in figure 10. The two configurations show almost identical qualitative performance with the side-feed unit giving consistently better performance. The side-feed-system discharge losses show more gradual increases with increasing ion-chamber potential differences (fig. 10(a)) when compared with the through-feed propellant-introduction mode. In this case, both propellant-introduction modes display an increase in energy dissipated in the discharge as the ion-chamber potential difference dropped below about 45 volts. Some increase in energy dissipated in the discharge with decreasing voltage is considered typical with most configurations, presumably because of the decreasing ionization cross section. This reduction in cross section requires higher emission currents to maintain a given propellant-utilization efficiency.

The variation of ion-chamber losses with increasing magnetic field shown in figure 10(b) is the same as that described in connection with the data obtained by using the first 10-centimeter-diameter thrustor (fig. 8(a), p. 9). The losses drop rapidly with field-strength increases to about 30 gauss and then level off. The side-feed propellant-introduction mode has lower losses when compared with the through-feed mode.

A comparison of the discharge energy losses with through- and side-feed propellant introduction with increasing net accelerating potential is shown in figure 10(c). The qualitative improvement in ion-chamber performance due to the increasing voltage is similar for both modes, while the side-feed unit gives lower discharge losses at a given voltage level.

The difference in absolute chamber-performance levels between the first (fig. 2, p. 4) and the second (fig. 3, p. 5) 10-centimeter-diameter thrustors was primarily due to the optimized magnetic-field configuration of the latter

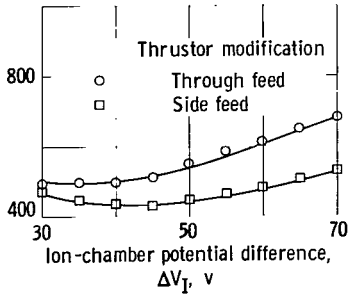

(a) Effect of ion-chamber potential difference on energy dissipated in ion-chamber discharge. Net accelerating potential, 4000 volts; magnetic-field strength at screen, 13 gauss.

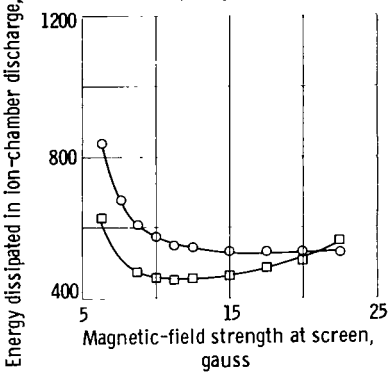

(b) Effect of magnetic-field strength at screen on energy dissipated in ion-chamber discharge. Net accelerating potential, 4000 volts; ion-chamber potential difference, 50 volts.

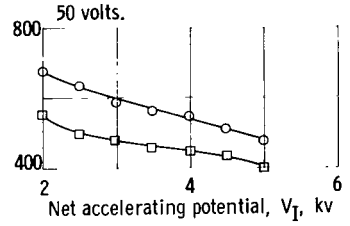

(c) Effect of net accelerating potential on energy dissipated in ion-chamber discharge. Ion-chamber potential difference, 50 volts; magnetic-field strength at screen, 13 gauss.

Figure 11. - Ion-chamber performance of 20-centimeter-diameter thrustor with through- and side-feed propellant introduction. Beam current, 0.5 ampere; accelerator potential, -2000 volts.

unit. This optimization had been accomplished in a previous program. Figures 7, 8, and 10 demonstrate that two thrustors of approximately the same dimensions but different absolute performance levels showed marked decreases in the energy dissipated in the ion-chamber discharge per beam ion when the location and the direction of the propellant flow into the ion chamber was changed.

Performance of 20-Centimeter-Diameter Source

The next series of tests was made with a 20-centimeter-diameter thrustor with through- and side-feed modes to determine the effect of scaling the size of the ion chamber. Figure 1 (p. 2) shows a cutaway view of the 20-centimeter-diameter thrustor in the through-feed configuration, and figure 4 (p. 6) shows a cutaway view of the side-feed unit.

The ion-chamber performance of these two thrustor modifications is shown in figure 11, where the energy dissipated in the ion-chamber discharge per beam ion is again compared for variations in ion-chamber potential difference, magnetic-field strength at the screen, and net accelerating potential.

The beam current was 0.5 ampere, which is the same average beam current density obtained with the 10-centimeter-diameter source at a beam current of 0.125 ampere.

The trends encountered with the 10-centimeter-diameter thrustors are again displayed in figure 11. The side-feed propellant-introduction mode again showed superior ion-chamber performance throughout the range of electrical parameters investigated.

The slight upturn in losses shown in figure 11(b) for the side-feed mode at magnetic-field strengths above 15 gauss is a departure from the typical level curve. This fact may be due to increased magnetic restraint of the energetic ionizing electrons, which prevents them from reaching the region near the periphery of the 20-centimeter-diameter thrustor, where high neutral density exists with side feed.

Data from the 20-centimeter-diameter thrustor are available in table III to construct a similar set of curves for both propellant-feed modes at a beam

current of 0.75 ampere.

An improvement in ion-chamber performance, such as that due to side feed, can increase either electrical-power efficiency or the propellant-utilization efficiency of a thrustor. For most applications, the product of these two terms, the overall thrustor efficiency, should be maximized. In reference 10 the overall thrustor efficiency for the standard 10 centimeter-diameter electron-bombardment thrustor is shown to have an optimum at a propellant-utilization efficiency of nearly 80 percent for the specific-impulse range investigated in this report (4000 to 5000 sec). The improved chamber performance of the side-feed modes (of the order of 25 percent) would allow a power efficiency or propellant-utilization efficiency increase of about 2 percent. The maximum overall thrustor efficiency would increase by a somewhat smaller percentage.

Beam-Current-Distribution Measurements

Beam-current-distribution profiles were taken with both the 10- and the 20-centimeter-diameter thrustors with side- and through-feed propellant-introduction modes. A movable 0.47-centimeter-diameter molybdenum disk 10 centimeters downstream of the thrustor was used as an impingement-current probe as it traversed the beam on the horizontal centerline of the thrustor, 12 centimeters downstream of the accelerator grids.

The anticipated improvement in uniformity of current distribution with the side-feed mode could not be verified with this probe positively because the quantitative variations in profile for the two modes were masked by the high sensitivity of the profiles to thrustor electrical parameters. As shown on the performance data plots (figs. 7 to 11, pp. 8 to 12), the effect of electrical parameters (i.e., discharge potential, magnetic field, and accelerating potential) gives ranges in discharge losses at least as large as does the change in propellant-introduction modes. In figure 7, for example, the range of discharge losses with varying ion-chamber potential is 300 to 500 electron volts per ion, while the performance of the through- and the cross-feed modes differ by less than 200 electron volts per ion. This effect also occurred in the beam-current-distribution measurements and obscured the sought-after profile variations due to propellant-introduction mode with large changes due to electrical parameters. The shapes of current-density traces taken with the 20-centimeter-diameter thrustor are shown in figure 12.

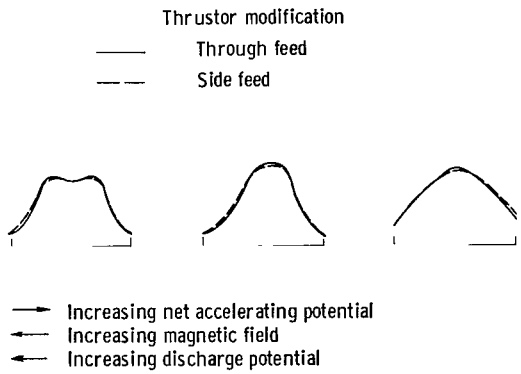

Figure 12. - Current-density traces of 20-centimeter-diameter thrustor.

Although the current-density profiles changed significantly with changes in electrical parameters, the variation with different feed modes was hard to distinguish. The electrode impingement current for all these traces remained nearly constant for each propellant-feed mode, as might be expected if the accelerator current was primarily due to charge-exchange ions.

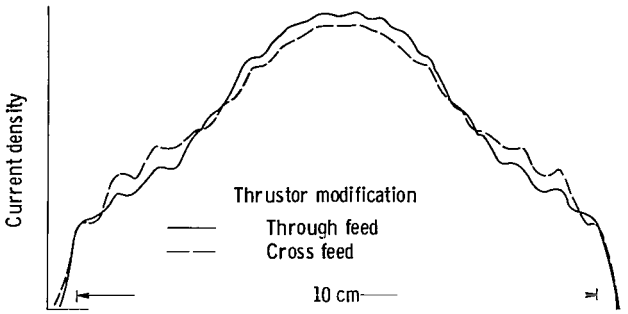

Figure 13. - Relative intensity of current density for 10-centimeter-diameter thrustor with through and cross feed. Beam current, 0.15 ampere; specific impulse, 5000 seconds; ion-chamber potential, 50 volts; magnetic-field strength, 33 gauss.

The distance from the probe to the accelerator grid was reduced from 12 to 1.5 centimeters to eliminate any effects on current distribution due to beam spread. Because of mounting clearances, traces could be taken only with the 10-centimeter-diameter thrustor (fig. 2, p. 4). A trace taken with the through-feed system is compared with one for the cross-feed mode in figure 13. The electrical parameters for both traces were the same and are recorded in figure 13. The small irregularities or bumps on the traces are due to the variations in current density as the probe passed through the individual beams from each accelerator grid hole. The cross-feed mode has a slightly better ion-current distribution than the through-feed mode.

A somewhat different quantitative picture of the current-density-distribution changes with different propellant-introduction modes was gained when a strip of tantalum 0.05 millimeter thick was fastened to the downstream face of the accelerator and covered a row of holes on the horizontal centerline of the thrustor. The unit was then operated at a constant point for 5 to 10 minutes to burn through the thin foil. The holes rapidly expanded until equilibrium was reached in 8 to 10 minutes. The condition was then held for periods up to 15 hours with no significant change in the size of the eroded hole. The variation of hole size could be estimated by observation with a small telescope and through decreases in impingement-current readings. The impingement current reached a static level, which was within a few percent of the normal accelerator impingement in about 10 minutes.

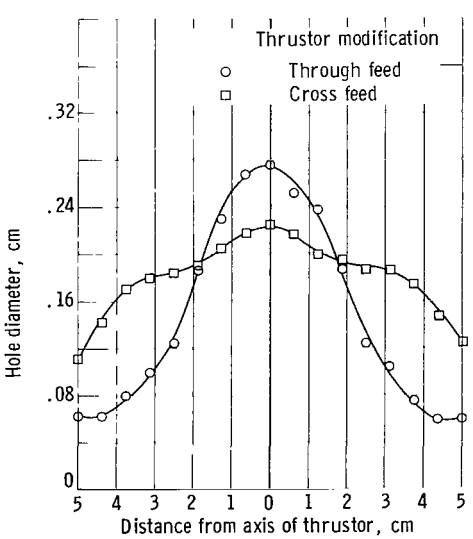

Figure 14. - Variation of eroded hole diameter with radius for through- and cross-feed propellant-introduction modes.

In figure 14 the diameters of the holes eroded in the foil by the ion beam are plotted against the distances of the holes from the axis of the thrustor. This test was performed with the first 10-centimeter-diameter thrustor by using both through- and cross-feed propellant introduction. The net accelerating potential was 4000 volts with the accelerator operating at -2000 volts; the beam current was 0.125 ampere. A 50-volt ion-chamber potential difference was used with a magnetic-field strength at the screen of 33 gauss.

Although this plot does not represent the ion-current distribution arriving at the plane of the accelerator, useful information can be inferred from it. With all electrical and physical parameters with the exception of the

propellant-feed mode held constant, it can probably be assumed that the similar-size holes at a radius of about 2 centimeters were eroded by qualitatively and quantitatively similar ion streams. If this test were to be performed with a theoretically "perfect" ion-source - accelerator-system combination, each eroded hole would be of the same diameter and would pass the same amount of current as every other hole. The plot then would appear as a horizontal line.

Figure 14 shows that the cross-feed unit is a better approximation to this ideal case than the through-feed unit. The reduced hole size of the cross-feed unit at the periphery of the thrustor may be due to wall losses (recombination) depleting the ion arrival rate at this radius, while the hump near the center is most probably due to unfocused (greater transverse velocity) ions that come from the more energetic plasma near the cathode.

Increasing the diameter of the anode beyond the outer radius of the accelerator holes should tend to increase the current flow in this area. The defocusing near the axis should be reduced by lowering the ion-chamber potential difference.

The variation of accelerator impingement with changes in propellant-introduction modes is much smaller than that caused by changes in electrical parameters such as net accelerating and/or accelerator potential. Inspection of the data indicates that the side-feed system had, on the average, a slightly lower accelerator-impingement current. All data were taken at beam-current densities at which the direct ion impingement current should be insignificant compared with the charge-exchange ion impingement current (ref. 2). Whether the slight decrease in the current intercepted by the accelerator is due to a decrease in the already small direct ion-impingement current or to a small reduction in charge-exchange ion current due to a redistribution of neutrals in the accelerator gap cannot be positively stated. The important change is in the distribution of the impingement current, which the accelerator-erosion measurements (fig. 14) indicate to be much more uniform for the side-feed system. The equations of reference 2 indicate that such increased uniformity could increase the life of the accelerator grids by as much as a factor of four over that obtained with a through-feed mode.

CONCLUDING REMARKS

Propellant introduction at the periphery of the ion chamber near the plane of the screen grid results in improved ion-chamber performance and more uniform accelerator erosion when compared with the conventional through-feed propellant-introduction mode. The postulated mechanisms for this improved chamber performance are more rapid extraction of ions formed in the region of high propellant density near the periphery of the chamber, an improved (more uniform) ion distribution arriving at the screen grid, and a longer mean neutral residence time in the chamber due to reduced initial-propellant-velocity components toward the 50-percent-open screen grid. The effect of the side-feed mode of propellant introduction on beam-current uniformity (and thus perhaps on

thrustor accelerator electrode durability) is more significant than the effect on thrustor efficiency.

Lewis Research Center,
National Aeronautics and Space Administration,
Cleveland, Ohio, October 13, 1964.

APPENDIX - SYMBOLS

J current, amp

P_M magnet power, coil resistance $\times (J_M)^2$

V potential, v

ΔV potential difference, v

Subscripts:

A accelerator

B beam

E emission

F filament

I ion chamber (anode)

M magnetic field

SD screen distributor

REFERENCES

1. Reader, Paul D.: An Electron-Bombardment Ion Rocket with a Permanent Magnet. AIAA Paper 63-031, March 1963. (Also in Astronautics and Aerospace Eng., vol. 1, no. 9, Oct. 1963, p. 83.)

2. Kerslake, William R.: Charge-Exchange Effects on the Accelerator Impingement of an Electron-Bombardment Ion Rocket. NASA TN D-1657, 1963.

3. Milder, Nelson L., and Kerslake, William R.: Evaluation of Filament Deterioration in Electron-Bombardment Ion Sources. NASA TN D-2173, 1964.

4. Sirois, William: Cathode Development Studies for Arc and Bombardment-Type Ion Engines. Rep. 34TR-073, NASA Contract NAS8-2513, Apr. 13, 1963. (Available from NASA (Attn: ATSS-AD), Washington, D.C. 20546.)

5. Kerslake, William R.: Cathode Durability in the Mercury Electron-Bombardment Ion Thrustor. AIAA Paper 64-683, 1964. (Also NASA TM X-52037.)

6. Kerslake, William R.: Accelerator Grid Tests on an Electron-Bombardment Ion Rocket. NASA TN D-1168, 1962.

7. Richley, Edward A., and Mickelsen, William R.: Effects of Molecular Flow in Plasma Generation and Some Analyses of Space Charge Flow in Ion Acceleration. AIAA Paper 64-7, 1964.

8. Kaufman, Harold R., and Reader, Paul D.: Experimental Performance of Ion Rockets Employing Electron-Bombardment Ion Sources. ARS Paper 1374-60, Nov. 1960. (Also in: Electrostatic Propulsion, Progress in Astronautics and Rocketry, vol. 5, David B. Langmuir, Ernst Stuhlinger, and J. M. Sellen, eds., Academic Press, New York, 1961, pp. 3-20.)

9. Reader, Paul D.: Investigation of a 10-Centimeter-Diameter Electron-Bombardment Ion Rocket. NASA TN D-1163, 1962.

10. Kaufman, Harold R.: The Electron-Bombardment Ion Rocket. In: Advanced Propulsion Concepts. Vol. 1. Gordon and Breach Science Publishers, Inc., New York, 1963, pp. 3-17.

TABLE I. - DATA OBTAINED WITH FIRST 10-CENTIMETER-DIAMETER SOURCE

[Magnet power, $P_M = 1.4\ (J_M)^2$ w; propellant-utilization efficiency, 0.8±0.05; filament power, 50 w/emitted amp; accelerator potential, -2000 v.]

(a) 0.125-Ampere beam

Ion-chamber potential difference, ΔV_I, v	Current collected by anode, J_I, amp	Current collected by accelerator, J_A, amp	Filament-emission current, J_E, amp	Magnetic-field current, J_M, amp	Magnetic-field strength at screen, gauss	Ion-chamber (net accelerating) potential, V_I, amp	Energy dissipated in discharge per beam ion, ev/ion	Ion-chamber potential difference, ΔV_I, v	Current collected by anode, J_I, amp	Current collected by accelerator, J_A, amp	Filament-emission current, J_E, amp	Magnetic-field current, J_M, amp	Magnetic-field strength at screen, gauss	Ion-chamber (net accelerating) potential, V_I, amp	Energy dissipated in discharge per beam ion, ev/ion
Through feed								Cross feed							
50	3.40	0.0008	2.90	2.0	18.5	2500	1310	50	4.50	0.0013	4.50	2.0	18.5	2500	1750
	2.65	.0007	2.30	2.5	23.2		1010		2.78	.0013	2.69	2.5	23.2		1060
	2.62	.0008	2.25	3.0	27.8		1000		2.19	.0013	2.00	3.0	27.8		827
	2.45		2.10	3.5	32.5		931		1.98	.0013	1.75	3.5	32.5		741
	2.35		2.00	4.0	37.1		892		1.87	.0014	1.65	4.0	37.1		699
	2.25		1.85	5.0	46.5		851		1.79		1.52	4.5	46.5		666
	2.18		1.83	6.0	55.7		822		1.72		1.51	5.0	55.7		638
	2.10		1.78	7.0	65.0		790		1.71		1.51	6.0	65.0		635
▼	2.05	▼	1.75	8.0	74.4	▼	770		1.70	▼	1.52	7.0	74.4		630
								▼	1.65	.0015	1.41	8.0		▼	610
75	2.45	.0008	1.70	3.5	32.5	2500	1400								
70	2.45	.0008	1.70				1300	75	1.68	.0013	1.38	3.5	32.5	2500	934
65	2.50	.0008	1.80				1235	70	1.70		1.40				882
60	2.70	.0008	2.00				1235	65	1.70		1.41				820
55	2.60	.0008	1.97				1090	60	1.80		1.53				805
50	2.70	.0009	2.20				1030	55	1.85		1.61				760
45	2.90	.0010	2.40				1000	50	2.00		1.80				750
40	2.90	.0010	2.50				888	45	2.05		1.90				693
35	3.10	.0010	2.80				832	40	2.32		2.30				702
30	3.45	.0011	3.45	▼	▼	▼	800	35	2.62		2.72				699
								30	3.20	▼	3.60	▼	▼	▼	738
50	2.59	.0013	2.40	3.5	32.5	2000	983								
	2.42	.0013	2.26			2500	919	50	2.15	.0016	2.00	3.5	32.5	2000	810
	2.37	.0013	2.15			3000	898		2.00	.0017	1.88			2500	750
	2.14	.0013	2.00			3500	805		1.92	.0018	1.79			3000	718
	2.14	.0013	1.97			4000	805		1.83	.0019	1.69			3500	682
	2.12	.0013	1.92			4500	796		1.78	.0020	1.60			4000	662
	1.98	.0013	1.80			5000	742		1.72	.0020	1.60			4500	638
	1.92	.0016	1.70			5500	720	▼	1.62	.0019	1.50	▼	▼	5000	598
▼	1.85	------	1.60	▼	▼	6000	690								
								40	3.90	.0015	4.00	2.0	18.5	4000	1208
40	4.87	.0013	4.59	1.5	13.9	4000	1515		2.55	.0014	2.50	2.5	23.2		776
	3.95	.0014	3.40	2.0	18.5		1222		2.15	.0015	2.10	3.0	27.8		648
	3.25	.0015	2.75	2.5	23.2		1000		2.09	.0016	2.00	3.5	32.5		629
	2.84	.0014	2.40	3.0	27.8		867		1.98	.0017	1.89	4.0	37.1		593
	2.50	------	2.20	3.5	32.5		760		1.90	.0017	1.82	4.5	41.8		568
	2.45	.0014	2.10	4.0	37.1		745		1.85	.0017	1.70	5.0	46.5		553
	2.28	.0014	1.92	4.5	41.8		690		1.80	.0017	1.70	6.0	55.7		536
	2.25	.0014	1.92	5.0	46.5		680		1.80	.0018	1.68	7.0	65.0		536
	2.15	------	1.89	6.0	55.7		648	▼	1.79	.0018	1.65	8.0	74.4	▼	535
▼	2.02	------	1.75	7.0	65.0	▼	606								
								75	1.48	.0020	1.22	3.5	32.5	4000	812
75	1.92	.0020	1.25	3.5	32.5	4000	1078	70	1.48	.0019	1.21				758
70	1.80	.0021	1.15				938	65	1.48	.0018	1.22				705
65	1.85	.0020	1.20				898	60	1.58	.0018	1.38				699
60	1.85	.0018	1.28				827	55	1.62		1.41				658
55	2.02	.0017	1.45				832	50	1.72		1.52				638
50	2.05	.0016	1.55				770	45	1.82		1.70				611
45	2.12	.0016	1.68				718	40	2.01		1.91				603
40	2.35	.0015	1.95				712	35	2.35	▼	2.40				623
35	2.42	.0014	2.12				642	30	2.89	.0017	3.10	▼	▼	▼	663
30	2.62	.0013	----	▼	▼	▼	600								

TABLE I. - Continued. DATA OBTAINED WITH FIRST 10-CENTIMETER-DIAMETER SOURCE

[Magnet power, $P_M = 1.4\ (J_M)^2$ w; propellant-utilization efficiency, 0.85±0.05; filament power, 50 w/emitted amp; accelerator potential, -2000 v.]

(a) Concluded. 0.128-Ampere beam

Ion-chamber potential difference, ΔV_I, v	Current collected by anode, J_I, amp	Current collected by accelerator, J_A, amp	Filament-emission current, J_E, amp	Magnetic-field current, J_V, amp	Magnetic-field strength at screen, gauss	Ion-chamber (net accelerating) potential, V_I, amp	Energy dissipated in discharge per beam ion, ev/ion	Ion-chamber potential difference, ΔV_I, v	Current collected by anode, J_I, amp	Current collected by accelerator, J_A, amp	Filament-emission current, J_E, amp	Magnetic-field current, J_M, amp	Magnetic-field strength at screen, gauss	Ion-chamber (net accelerating) potential, V_I, amp	Energy dissipated in discharge per beam ion, ev/ion
	Angle feed								Reverse feed						
50	3.21	0.0014	3.10	2.0	16.5	2500	1232	50	1.56	0.0012	1.20	8.0	16.5	2500	574
	1.95	.0014	1.75	2.5	23.2		730		1.57	------	1.20	7.0	23.2		577
	1.80	.0013	1.61	3.0	27.8		670		1.55	.0012	1.20	6.0	27.8		570
	1.70	.0012	1.50	3.5	32.5		630		1.61	.0012	1.25	5.0	32.5		592
	1.61	.0013	1.41	4.0	37.1		594		1.62	------	1.28	4.5	37.1		597
	1.60	.0013	1.39	4.5	41.8		590		1.62	.0012	1.32	4.0	41.8		597
	1.59	.0013	1.38	5.0	46.4		586		1.75	.0012	1.40	3.5	46.4		650
	1.51	.0013	1.31	6.0	55.7		553		1.65	------	1.55	3.0	55.7		690
	1.51	.0013	1.31	7.0	65.0		553		2.15	.0012	1.90	2.5	65.0		810
	1.50	.0013	1.30	8.0	74.4		550		2.70	------	2.45	2.0	74.4		1030
75	1.60	.0013	1.32	3.5	32.5	2500	885	75	1.52	.0011	1.17	3.5	32.5	2500	836
70	1.62		1.32				837	70	1.58	.0010	1.20				813
65	1.65		1.40				793	65	1.58	.0010	1.22				755
60	1.69		1.42				751	60	1.62		1.26				718
55	1.75		1.50				715	55	1.70		1.35				692
50	1.83		1.60				682	50	1.75		1.45				650
45	1.90		1.70				639	45	1.85		1.65				632
40	2.12	.0012	2.00				639	40	2.02		1.80				606
35	2.31	.0012	2.29				614	35	2.15		1.98				567
30	2.79	.0012	2.98				841	30	2.80		2.45				570
50	2.12	.0015	2.00	3.5	32.5	2000	798	50	1.95	.0010	1.67	3.5	32.5	2000	742
	2.00	.0014	1.89			2500	750		1.80	.0009	1.55			2500	670
	1.89		1.79			3000	706		1.72	.0010	1.42			3000	638
	1.75		1.62			3500	650		1.65		1.39			3500	610
	1.70		1.51			4000	630		1.60		1.30			4000	590
	1.60		1.48			4500	590		1.55		1.20			4500	582
	1.59		1.40			5000	586		1.48		1.15			5000	542
									1.40		1.08			6000	510
40	3.68	.0013	3.70	2.0	18.5	4000	1175								
	2.30		2.20	2.5	23.2		696	40	1.57	.0011	1.31	7.0	65.0	4000	462
	1.95		1.85	3.0	27.8		584		1.59	.0011	1.30	6.0	55.7		468
	1.81		1.71	3.5	32.5		538		1.62	.0010	1.36	5.0	46.4		476
	1.75		1.60	4.0	37.1		520		1.67		1.40	4.5	41.8		494
	1.70		1.59	4.5	41.8		504		1.70		1.42	4.0	37.1		503
	1.72	.0014	1.61	5.0	46.4		510		1.73		1.52	3.5	32.5		512
	1.72	.0015	1.61	6.0	55.7		510		1.85		1.62	3.0	27.8		552
	1.65	.0015	1.58	7.0	65.0		488		1.96		1.80	2.5	23.2		587
	1.62	.0015	1.55	8.0	74.4		478		3.00		2.92	2.0	18.5		920
75	1.42	.0018	1.02	3.5	32.5	4000	777	75	1.33	.0010	0.96	3.5	32.5	4000	723
70	1.50		1.20				770	70	1.35		.99				685
65	1.50		1.21				715	65	1.38		1.08				652
60	1.55		1.30				683	60	1.43		1.10				627
55	1.60		1.35				648	55	1.52		1.22				612
50	1.75		1.55				650	50	1.56		1.28				582
45	1.82		1.69				610	45	1.67		1.40				556
40	2.00		1.90				600	40	1.81		1.59				538
35	2.22	.0017	2.22				586	35	1.98		1.82				520
30	2.59	.0017	2.79				591	30	2.23		2.20				506
								25	2.95		3.17				566

TABLE I. - Concluded. DATA OBTAINED WITH FIRST 10-CENTIMETER-DIAMETER SOURCE

[Magnet power, $P_M = 1.4\ (J_M)^2$ w; propellant-utilization efficiency, 0.8±0.05; filament power, 50 w/emitted amp; accelerator potential, -2000 v.]

(b) 0.25-Ampere beam

Ion-chamber potential difference, ΔV_I, v	Current collected by anode, J_I, amp	Current collected by accelerator, J_A, amp	Filament-emission current, J_E, amp	Magnetic-field current, J_M, amp	Magnetic-field strength at screen, gauss	Ion-chamber (net accelerating) potential, V_I, amp	Energy dissipated in discharge per beam ion, ev/ion
Through feed							
50	3.90	0.0132	2.98	8.0	74.4	4000	730
	3.72	.0084	2.80	7.0	65.0		694
	3.90	.0065	3.00	6.0	55.7		730
	4.13	.0050	3.20	5.0	46.5		776
	4.25	.0040	3.30	4.5	41.8		800
	4.60	.0031	3.60	4.0	37.1		870
	4.70	.0032	3.60	3.5	32.5		890
▼	5.00	.0032	3.90	3.0	27.8	▼	950
75	4.30	.0046	2.90	4.5	41.8	4000	1215
70	4.30	.0045	2.98				1135
65	4.60	.0045	3.30				1130
60	4.50	.0045	3.30				1020
55	4.65	.0044	3.55				968
50	4.65	.0044	3.70				880
45	5.0	.0047	4.15	▼	▼	▼	852
50	3.73	.0042	2.90	4.5	41.8	7000	696
	4.02	.0042	3.20			6500	754
	4.18	.0042	3.30			6000	785
	4.25	.0042	3.38			5500	800
	4.42	.0043	3.50			5000	834
	4.70	.0044	3.75			4500	890
	4.78	.0044	3.78			4000	906
▼	5.00	.0052	4.00	▼	▼	3500	950
Angle feed							
50	3.55	0.0060	2.65	8.0	74.4	4000	660
	3.55	.0051	2.85	7.0	65.0		660
	3.60	.0049	2.85	6.0	55.7		670
	3.70	.0048	3.00	5.0	46.5		690
	3.80	.0047	3.20	4.5	41.8		710
	3.85	.0046	3.25	4.0	37.1		720
	4.20	.0046	3.65	3.5	32.5		790
▼	4.45	.0045	3.95	3.0	27.8	▼	840
75	3.20	.0048	2.30	4.5	41.8	4000	885
70	3.20	.0047	2.35				826
65	3.20	.0046	2.45				767
60	3.30	.0045	2.55				732
55	3.45	.0045	2.75				704
50	3.60	.0045	3.00				670
45	3.90	.0045	3.30				657
40	4.30	.0043	3.80				648
35	4.60	.0044	4.25	▼	▼	▼	610
50	3.45	.0043	2.80	4.5	41.8	4500	640
▼	3.65	.0044	3.10	▼	▼	4000	680
	3.90	.0044	3.30			3500	730
Cross feed							
50	3.75	0.0047	2.85	8.0	74.4	4000	700
	3.90	.0047	3.00	7.0	65.0		730
	3.90	.0045	3.00	6.0	55.7		730
	3.92	.0044	3.05	5.0	46.5		735
	4.10	.0044	3.25	4.5	41.8		770
	4.15	.0042	3.32	4.0	37.1		780
	4.45	.0042	3.65	3.5	32.5		840
	4.80	.0041	4.05	3.0	27.8		910
▼	5.00	.0041	4.30	2.7	25.1	▼	950
70	3.42	.0048	2.50	4.5	41.8	4000	888
65	3.50	.0046	2.60				845
60	3.60	.0044	2.63				804
55	3.82	.0044	2.90				786
50	4.08	.0043	3.25				767
45	4.30	.0043	3.50				729
40	4.90	.0042	4.22	▼	▼	▼	744
50	3.41	.0039	2.69	4.5	41.8	7000	632
	3.60	.0040	2.88			6500	670
	3.70	.0040	2.92			6000	690
	3.78	------	2.92			5500	706
	3.90	.0042	3.05			5000	730
	3.95	.0042	3.10			4500	740
	4.00	.0042	3.15			4000	750
▼	4.10	.0042	3.28	▼	▼	3500	770
Reverse feed							
50	3.50	0.0065	2.70	8.0	74.4	4000	650
	3.45	.0057	2.70	7.0	65.0		640
	3.50	.0055	2.80	6.0	55.7		650
	3.60	.0055	3.00	5.0	46.5		670
	3.67	.0054	3.05	4.5	41.8		684
	3.81	.0052	3.18	4.0	37.1		712
	4.02	.0051	3.40	3.5	32.5		754
	4.45	.0050	3.90	3.0	27.8		840
▼	5.45	.0050	4.90	2.5	23.2	▼	1040
75	3.20	.0057	2.30	4.5	41.8	4000	886
70	3.28	.0053	2.40				846
65	3.30	.0050	2.45				794
60	3.30	.0051	2.50				732
55	3.47	.0050	2.70				708
50	3.70	.0051	3.00				690
45	3.90		3.30				657
40	4.25		3.70				640
35	4.70	▼	4.35	▼	▼	▼	623
50	3.50	------	2.85	4.5	41.8	5000	650
	3.75	.0055	3.00			4500	700
	3.85	.0053	3.20			4000	720
▼	4.05	.0053	3.35	▼	▼	3500	760

TABLE II. - DATA OBTAINED WITH SECOND 10-CENTIMETER-DIAMETER SOURCE

[Beam current, 0.125; magnet power, $P_M = 1.0 (J_M)^2$ w; propellant-utilization efficiency, 0.8±0.05; filament power, 50 w/emitted amp; accelerator potential, -2000 v.]

Ion-chamber potential difference, ΔV_I, v	Current collected by anode, J_I, amp	Current collected by accelerator, J_A, amp	Filament-emission current, J_E, amp	Magnetic-field current, J_M, amp	Magnetic-field strength at screen, gauss	Ion-chamber (net accelerating) potential, V_I, amp	Energy dissipated in discharge per beam ion, ev/ion	Ion-chamber potential difference, ΔV_I, v	Current collected by anode, J_I, amp	Current collected by accelerator, J_A, amp	Filament-emission current, J_E, amp	Magnetic-field current, J_M, amp	Magnetic-field strength at screen, gauss	Ion-chamber (net accelerating) potential, V_I, amp	Energy dissipated in discharge per beam ion, ev/ion
			Through feed								Side feed				
50	1.82	0.00090	1.48	8.0	61.0	2500	678	50	1.38	0.00100	1.15	8.0	61.0	2500	502
	1.75	.00085	1.40	7.0	53.3		650		1.38	.00100	1.15	7.0	53.3		502
	1.80	.00082	1.42	6.0	45.6		670		1.38	.00100	1.14	6.0	45.6		502
	1.80	.00082	1.42	5.0	38.0		670		1.40	.00100	1.16	5.0	38.0		510
	1.85	.00080	1.45	4.5	34.3		690		1.40	.00100	1.16	4.5	34.3		510
	1.89	.00082	1.49	4.0	30.5		706		1.42	.00095	1.16	4.0	30.5		518
	1.95	.00075	1.52	3.5	26.6		730		1.43	.00095	1.18	3.5	26.6		522
	2.18	.00080	1.70	3.0	22.8		822		1.42	.00095	1.38	3.0	22.8		558
	2.60	.00080	2.12	2.5	19.0		990		1.78	.00090	1.50	2.75	21.0		662
									2.00	.00100	1.75	2.5	19.0		750
75	1.55	-------	.87	4.0	30.5	2500	855		2.18	.00100	1.95	2.25	17.1		810
70	1.55	.00130	.92				798		2.48	.00095	2.25	2.0	15.2		930
65	1.57	-------	.98				752								
60	1.62	-------	1.02				718	75	1.12	.00145	.78	4.0	30.5	2500	597
55	1.68	.00120	1.12				683	70	1.18	.00130	.80				590
50	1.70	.00115	1.20				630	65	1.22	.00140	.85				569
45	1.82	.00105	1.40				610	60	1.20	.00142	.85				516
40	1.88	.00105	1.52				562	55	1.29	.00113	1.00				512
35	2.18	.00095	1.95				575	50	1.42	.00135	1.12				517
30	2.90	.00095	2.80				666	45	1.52	.00130	1.30				502
								40	1.72	.00110	1.53				510
40	2.98	.00085	2.62	2.0	15.2	4000	913	35	2.02	.00135	1.95				531
	2.25	.00070	1.93	2.5	19.0		680	30	2.90	.00130	2.90				666
	2.00	.00085	1.70	3.0	22.8		600								
	1.90	.00085	1.58	3.5	26.6		568	40	3.38	.00100	3.38	1.5	11.4	4000	1040
	1.81	.00080	1.51	4.0	30.5		539		2.60	.00095	2.50	2.0	15.2		792
	1.80	.00085	1.50	4.5	34.3		535		1.95	-------	1.80	2.5	19.0		584
	1.82	.00085	1.52	5.0	38.0		542		1.73	.00090	1.60	3.0	22.8		514
	1.82	.00085	1.58	6.0	45.6		542		1.62	-------	1.48	3.5	26.6		479
	1.82	.00085	1.61	7.0	53.3		542		1.56	.00085	1.43	4.0	30.5		459
									1.51	-------	1.42	4.5	34.3		456
75	1.50	.00085	.90	4.0	30.5	4000	825		1.57	.00085	1.45	5.0	38.0		462
70	1.50	.00085	.92				771		1.55	-------	1.45	6.0	45.6		456
65	1.52	.00085	1.00				726		1.55	.00080	1.45	7.0	53.3		456
60	1.53	.00085	1.02				675								
55	1.59	.00085	1.12				645	75	1.05	.00085	.75	4.0	30.5	4000	555
50	1.70	.00085	1.30				630	70	1.10	.00077	.82				546
45	1.75	.00085	1.40				585	65	1.12	.00075	.89				518
40	2.00	.00085	1.75				600	60	1.20	.00072	.91				516
35	2.72	.00080	2.55				727	55	1.22		.98				482
								50	1.30		1.08				470
50	2.00	.00090	1.56	4.0	30.5	2000	750	45	1.40		1.20				459
	1.82	.00085	1.42			2500	678	40	1.65	.00070	1.52				488
	1.78	.00085	1.35			3000	662	35	2.28	.00070	2.30				603
	1.76	.00082	1.35			3500	654								
	1.70	-------	1.30			4000	630	50	1.53	.00075	1.30	4.0	30.5	2000	562
	1.62	.00085	1.25			4500	597		1.45	-------	1.22			2500	530
	1.58	.00090	1.20			5000	581		1.42	.00070	1.18			3000	518
									1.39	-------	1.15			3500	506
									1.30	-------	1.05			4000	470
									1.22	-------	1.00			5000	438

TABLE III. - DATA OBTAINED WITH 20-CENTIMETER-DIAMETER SOURCE

[Magnet power, $P_M = 0.85\ (J_M)^2$ w; propellant-utilization efficiency, 0.8±0.05; filament power, 50 w/emitted amp; accelerator potential, -2000 v.]

(a) Beam current, 0.50 ampere

Ion-chamber potential difference, ΔV_I, v	Current collected by anode, J_I, amp	Current collected by accelerator, J_A, amp	Filament-emission current, J_E, amp	Magnetic-field current, J_M, amp	Magnetic-field strength at screen, gauss	Ion-chamber (net accelerating) potential, V_I, amp	Energy dissipated in discharge per beam ion, ev/ion	Ion-chamber potential difference, ΔV_I, v	Current collected by anode, J_I, amp	Current collected by accelerator, J_A, amp	Filament-emission current, J_E, amp	Magnetic-field current, J_M, amp	Magnetic-field strength at screen, gauss	Ion-chamber (net accelerating) potential, V_I, amp	Energy dissipated in discharge per beam ion, ev/ion
	Through feed								Side feed						
50	5.80	0.0043	4.50	18.0	22.5	4000	530	50	6.15	0.0048	5.00	18.0	22.5	4000	565
	5.90	.0041	4.52	16.0	20.0		540		5.60	.0046	4.20	16.0	20.0		510
	5.85	.0039	4.45	14.0	17.5		535		5.40	.0042	4.10	14.0	17.5		490
	5.85	.0037	4.35	12.0	15.0		535		5.15	.0039	3.80	12.0	15.0		465
	5.95	.0035	4.45	10.0	12.5		545		5.10	.0038	3.85	10.0	12.5		460
	6.00	.0035	4.40	9.0	11.3		550		5.08	.0036	3.70	9.0	11.3		458
	6.30	.0033	4.65	8.0	10.0		580		5.15	.0035	3.90	8.0	10.0		465
	6.60		4.85	7.0	8.8		610		5.25	.0035	3.95	7.0	8.8		475
	7.30		5.50	6.0	7.5		680		----	.0034	----	6.0	7.5		---
	8.90		6.90	5.0	6.3		840		6.80	.0033	5.65	5.0	6.3		630
70	5.35	.0034	3.40	10.0	12.5	4000	679	70	4.30	.0035	2.85	10.0	12.5	4000	532
65	5.49	.0034	3.52				649	65	4.40	.0035	3.05				507
60	5.60	.0033	3.80				612	60	4.50	.0035	3.15				480
55	5.83	.0033	4.10				587	55	4.70	.0034	3.40				462
50	6.00	.0033	4.40				550	50	5.00	.0033	3.80				450
45	6.18	.0032	4.70				512	45	5.30	.0034	4.30				432
40	6.70	.0032	5.50				496	40	5.95	.0033	5.10				436
35	7.60	.0031	6.60				497	35	6.90	.0033	6.40				448
30	8.70	.0032	8.40				492	30	8.30	.0033	8.70				468
50	7.28	.0038	5.40	10.0	12.5	2000	678	50	6.05	------	4.60	10.0	12.5	2000	555
	6.85	.0036	5.10			2500	635		5.45	.0037	4.15			2500	495
	6.35	.0034	4.70			3000	585		5.29	.0035	4.00			3000	479
	6.12	.0032	4.45			3500	562		5.10	.0033	4.00			3500	460
	6.00	.0031	4.40			4000	550		5.00	.0032	3.80			4000	450
	5.67	.0031	4.10			4500	517		4.90	.0032	3.65			4500	440
	5.28	.0031	3.88			5000	478		4.50	.0032	3.38			5000	400
65	6.50	.0090	4.20	10.0	12.5	2500	780	65	4.78	.0050	3.15	10.0	12.5	2500	556
60	6.50	.0070	4.40				719	60	5.20	.0053	3.65				564
55	6.70	.0053	4.80				682	55	5.70	.0052	4.05				572
50	6.90	.0050	5.10				640	50	6.00	.0052	4.42				550
45	7.10	.0048	5.45				594	45	6.45	.0050	4.90				535
40	7.70	.0047	6.30				576	40	7.00	.0048	5.80				520
35	8.50	.0046	7.50				560	35	7.80	.0045	6.90				511

(b) Beam current, 0.7 ampere

50	10.7	0.0240	8.4	20.0	25.0	4000	664	50	11.0	0.0205	8.8	20.0	25.0	4000	683
	10.3	.0180	7.9	18.0	22.5		637		10.3	.0170	7.8	18.0	22.5		636
	10.4	.0130	7.5	16.0	20.0		643		9.6	.0130	7.1	16.0	20.0		590
	10.6	.0120	8.0	14.0	17.5		656		9.4	.0130	6.9	14.0	17.5		577
	10.8	.0120	8.0	12.0	15.0		670		9.3	.0122	6.8	12.0	15.0		570
	11.0	.0115	8.1	10.0	12.5		684		9.2	.0118	6.8	10.0	12.5		563
	11.6		8.5	9.0	11.3		723		9.5	.0113	7.4	9.0	11.3		583
	12.2		9.0	8.0	10.0		764		10.2	.0113	8.0	8.0	10.0		630
	13.9		10.4	7.0	8.8		676		11.4	.0112	9.5	7.0	8.8		710
									14.6	.0108	12.7	6.0	7.5		923
70	9.5	.0133	6.0	11.5	14.4	4000	817								
65	9.6	.0138	6.3				766	70	8.1	.0115	5.4	11.5	14.4	4000	686
60	10.0	.0136	6.8				740	65	8.3	.0114	5.5				655
55	10.5	.0130	7.5				715	60	8.5	.0112	6.0				620
50	10.5	.0125	7.7				650	55	8.9	.0111	6.4				597
45	11.0	.0130	8.5				615	50	9.3	.0111	6.9				571
40	11.5	.0133	9.3				574	45	9.7	.0107	7.5				537
32	12.4	.0150	10.8				497	40	10.4	.0105	8.6				515
								35	12.0	.0103	10.8				525
40	11.5	.0133	9.3	11.5	14.4	4000	574								
40	12.5	.0178	10.3	11.5	14.4	3600	627	40	11.6	.0109	9.9	11.5	14.4	3000	578
									11.1	.0105	9.3			3500	552
									10.7	.0102	8.9			4000	531
									10.2	.0099	8.5			4500	505
									9.8	.0095	8.1			5000	483

"The aeronautical and space activities of the United States shall be conducted so as to contribute . . . to the expansion of human knowledge of phenomena in the atmosphere and space. The Administration shall provide for the widest practicable and appropriate dissemination of information concerning its activities and the results thereof."

—NATIONAL AERONAUTICS AND SPACE ACT OF 1958

NASA SCIENTIFIC AND TECHNICAL PUBLICATIONS

TECHNICAL REPORTS: Scientific and technical information considered important, complete, and a lasting contribution to existing knowledge.

TECHNICAL NOTES: Information less broad in scope but nevertheless of importance as a contribution to existing knowledge.

TECHNICAL MEMORANDUMS: Information receiving limited distribution because of preliminary data, security classification, or other reasons.

CONTRACTOR REPORTS: Technical information generated in connection with a NASA contract or grant and released under NASA auspices.

TECHNICAL TRANSLATIONS: Information published in a foreign language considered to merit NASA distribution in English.

TECHNICAL REPRINTS: Information derived from NASA activities and initially published in the form of journal articles.

SPECIAL PUBLICATIONS: Information derived from or of value to NASA activities but not necessarily reporting the results of individual NASA-programmed scientific efforts. Publications include conference proceedings, monographs, data compilations, handbooks, sourcebooks, and special bibliographies.

Details on the availability of these publications may be obtained from:

SCIENTIFIC AND TECHNICAL INFORMATION DIVISION

NATIONAL AERONAUTICS AND SPACE ADMINISTRATION

Washington, D.C. 20546